https://doi.org/10.48048/tis.2024.8050

# Derivative Analysis of Gravity Data in Revealing the Subsurface Fault Structure Model in Semeru Volcano, East Java and Its Surrounding

**Laily Nur Hofi[1], Sukir Maryanto[1,2,*], Adi Susilo[1] and Sri Dwi Wuryani[2]**

*[1]Department of Physics, Faculty of Mathematics and Natural Science, Brawijaya University, Jawa Timur 65145, Indonesia*
*[2]Brawijaya Volcanology and Geothermal Research Center, Brawijaya University, Jawa Timur 65145, Indonesia*

**([*]Corresponding author's email: sukir@ub.ac.id)**

*Received: 7 February 2024, Revised: 4 March 2024, Accepted: 27 March 2024, Published: 10 August 2024*

**Abstract**

Research with gravity data in the area of Semeru volcano has been undertaken. The study aims to determine the subsurface fault structure of the Semeru volcano by utilizing derivative analysis of gravity data anomalies. A comprehensive dataset of 1,929 measurement points, spaced 500 m apart, was analyzed to identify variations in the Bouguer anomaly. Complete Bouguer anomaly values ranged from 37 to 111 mGal. The contrast of Bouguer anomaly variations effectively delineates the boundaries of different rock formations: Mandalika, Wuni, Quarter Volcanic Semeru and Quarter Volcanic Jembangan. These formations are instrumental in causing significant variations in gravity anomalies, indicating an underlying geological structure. The derivative analysis, encompassing horizontal (FHD) and vertical (SVD) anomalies, unveiled a pronounced fault structure southeast of the Semeru crater, characterized by a NE-SW orientation. Advanced modeling, informed by residual anomaly incision lines and depth estimates derived from the radial spectrum, revealed a complex subsurface stratigraphy consisting of 5 types: Volcanic clastics, tuff, breccia, basaltic lava and andesitic lava. This research advances our understanding of the Semeru volcano's subsurface architecture. It introduces an enhanced methodology for fault detection and characterization in volcanic areas, showcasing the potential of gravity data in geological investigations.

**Keywords:** Gravity, FHD, SVD, Subsurface fault structure, Semeru volcano

## Introduction

Modeling the subsurface structure is vital for understanding tectonic activity and seismic risk [1,2]. Movement within geological structures, local and regional faults, can create zones of weak ground, triggering movements that manifest as earthquakes and landslides [3,4]. Subduction earthquakes sometimes result in significant destruction within the fault zones [5]. For example, in Pohgajih, Malang, numerous homes were damaged directly atop a fault's location [6]. Similarly, in China, faults primarily governed the spread of landslides post-earthquakes [7].

East Java, located along the southwestern boundary of the Eurasian Plate within the Sunda Arc, experiences orthogonal subduction above the Indo-Australian Plate [8,9]. This geographical location can trigger a high seismicity risk, typically ranging in magnitudes from 4.8 to 5.5 [10]. In addition, the

volcanoes in East Java play a significant role in the region's seismicity [11]. Semeru volcano is the highest volcano in Java [12] and one of the most active lava producers [13]. The occurrence of damage from the effects of volcanoes and tectonics cannot be prevented, but its impact can be minimized through effective mitigation and reduction of vulnerability. A key strategy involves identifying subsurface geological structures, including fault detection, and determining the types of rock formation in the subsurface. Therefore, a comprehensive understanding and monitoring of these geological structures is vital for developing the disaster awareness and response plans in East Java.

Various gravity techniques have illustrated the subsurface, with past research [14-16] employing gravity methods to detect the location of faults, determine the type of faults [17,18], and model the fault structures of Lawu Volcano [19], demonstrating gravity data's efficacy in estimating rock layer depths [20]. Nonetheless, few studies have focused on integrating detailed fault structure mapping with extensive rock formation analysis in the Semeru region. The complexity of subsurface geological features, compounded by steep terrain, presents obstacles to the direct acquisition methods [21], especially for large-scale modeling efforts. There remains a need for a more efficient approach to obtaining detailed subsurface information. These limitations highlight the importance of exploring alternative approaches, such as utilizing gravity satellite data to determine the subsurface structure. According to Suprianto *et al.* [22], satellite gravity data is known for its high resolution. Gravity data consist of latitude, altitude and free air anomaly [23,24], marking it less susceptible to subsurface interference than ground-based measurements, which may be affected by local topography variations and instrument use inaccuracies. Thus, gravity data provide a more consistent source of information for accurately characterizing and interpreting subsurface structures.

The gravity data are commonly used to detect rock formations based on Bouguer anomaly and gravity field variations [25]. The distribution of Bouguer anomalies is related to local variations, which refer to deep anomalies. Accordingly, the gravity methods provide a clear vision of the subsurface geological structure and rock density distribution. Geological structure can trigger the contrast of density in the fault zone [26,27]. In particular, the analysis derivative, First Horizontal Derivative (FHD) and Second Vertical Derivate (SVD) can detect the contrast change of Bouguer anomaly in the subsurface. Offering detailed insights into subsurface geological geometries [28]. FHD shows the difference in the anomaly value of geological boundaries horizontally [29]. Meanwhile, SVD distinguishes between shallow and regional anomalies, helping to delineate geological structure boundaries. It has a high absolute value on the FHD map curve and a value of 0 mGal/km (0 isoline) on the SVD map curve [1]. Thus, the FHD and SVD curves will validate each other when a fault is along the derivative line [30]. Detailed research will use gravity to estimate subsurface geological structures and Bouguer anomaly discontinuities that indicate faults. The results of this study are expected to be a reference for subsurface structure research in areas dominated by faults and fractures.

## Materials and methods

### Geology of study area

Semeru volcano is located between Lumajang Regency and Malang Regency in East Java. The volcano is highest in Java, with Semeru being the compound cone that forms its highest peak [31,32]. The topography of the Semeru volcano ranges from an altitude of 490 to 3,676 m above sea level with UTM coordinate boundaries, the boundaries of which research area are shown in **Figure 1**. This volcano is a composite volcano that is still active and one of the most prolific producers of lavas [33,34].

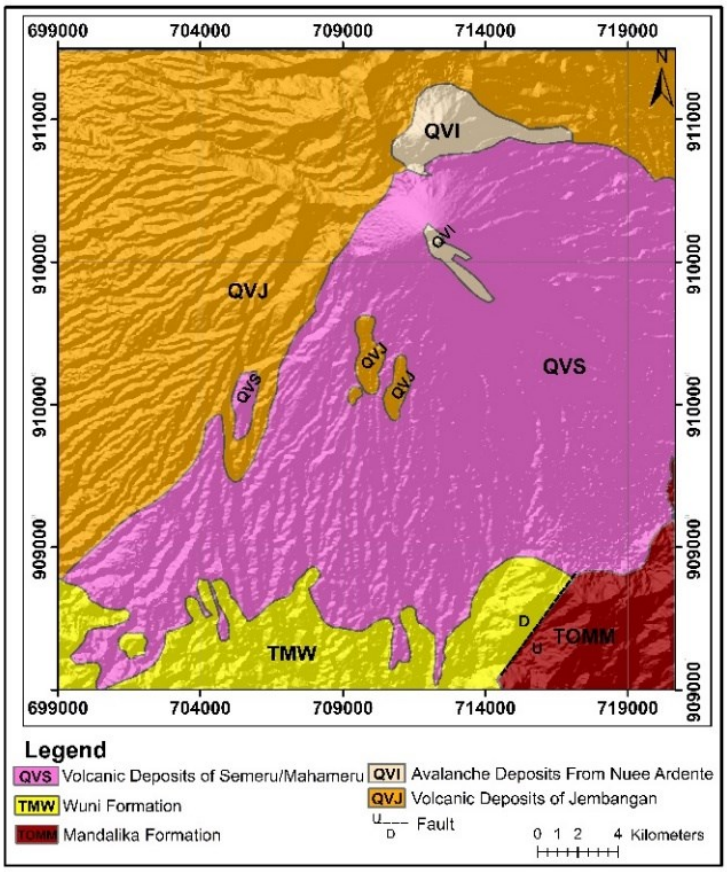


**Figure 1** The geological map of the Semeru composite cone is based on the geological map [35]. Displaying stratigraphic unit for easy identification.

Based on **Figure 1**, Semeru rock formations consist of Wuni, Mandalika, Semeru volcanic deposits as well as volcanic deposits of Jembangan [35]. The contact boundaries of these formations at the volcano facilitate the development of geological structures, including geological contacts and local faults [36]. In this research, the subsurface fault structure geophysical methods to map the distribution of anomalies associated with Semeru volcano. This subsurface structure model includes the type of rock, the rock formation's thickness and the fault structure's illustration.

**Gravity**

The gravity satellite data extraction in this research utilizes the Global Gravity Model plus (GGMplus) as a preliminary exploration tool to measure the subsurface structures with optimal resolution and large-scale measurement coverage [18]. GGMplus integrates data from various sources, including the GRACE (Gravity Recovery and Climate Experiment), GOCE (Gravity field and steady-state Ocean Circulation Explorer), EGM 2008 (Earth Gravity Model) and the gravitational topography effects, to improve resolution through integration [37]. The dataset allows for spaces up to 500 m between measurement points. Data processing to determine the subsurface fault structure in Semeru volcano used 1,937 data extraction points.

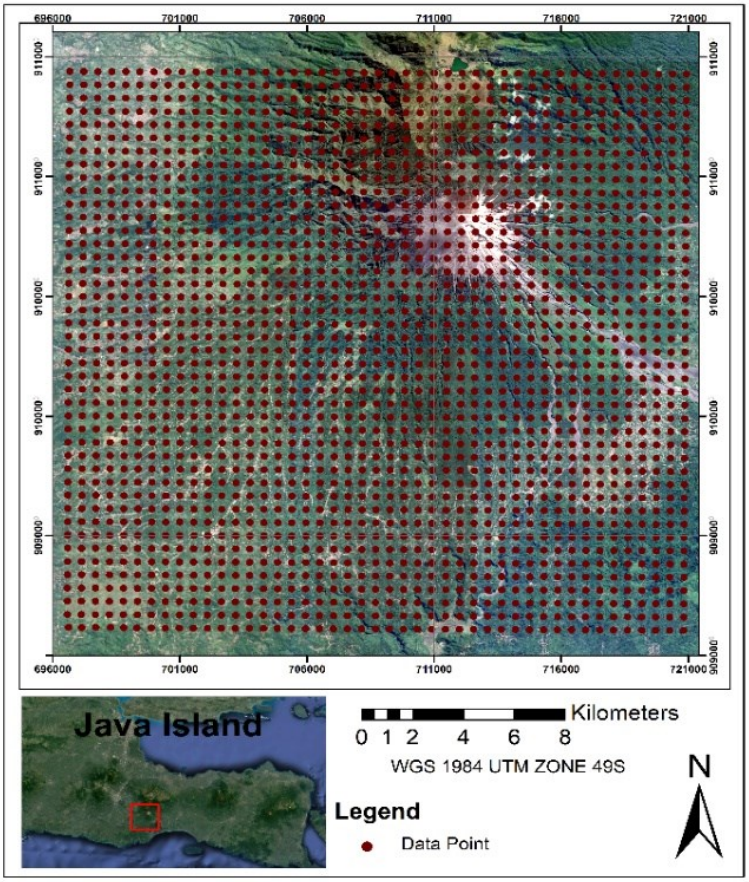


**Figure 2** Research map design (this figure was made using Google Earth map). The red point donates the locations of gravity satellite data points.

The GGMplus gravity satellite data was downloaded from the website https://murray-lab.caltech.edu/GGMplus/index.html, in Text Document (.txt) format, includes disturbance gravity information and can be processed using Microsoft Office Excel. Elevation data necessary for processing can be obtained from https://earthexplorer.usgs.gov/. Processing involved using Microsoft Office Excel to correct the data, converting raw gravity readings to free-air anomalies, necessitating Bouguer and terrain corrections to obtain the complete Bouguer anomaly [38]. The Complete Bouguer Anomaly (CBA) will be transformed into a flat plane to minimize distortion and for more straightforward data interpretation [39]. The subsequent step involves applying an upward continuation filter to transform potential field data from a specific surface to a perceived higher surface level. Upward continuation also serves to eliminate noise from near-surface objects. The field reduction process distinguishes regional and residual anomalies, separating them based on the radial average power spectrum value [40]. Regional anomalies denote gravity anomalies indicative of deep rock distributions. Residual anomalies represent rock distribution in shallow areas. The residual anomaly data obtained is then subjected to derivative analysis. The Derivative analysis involves plotting fault structures, encompassing the First Horizontal Derivative (FHD) and Second Vertical Derivative (SVD). The calculation discrete approximation of the analysis derivative along the x-axis [41] is shown in the equation:

$$FHD = \left(\frac{\partial g}{\partial x}\right)(x_n, y_n) = \sqrt{\left(\frac{\partial g}{\partial x}\right)^2 + \left(\frac{\partial g}{\partial y}\right)^2} \quad (1)$$

$$SVD = \frac{\partial^2 g}{\partial z^2} = -\left(\frac{\partial^2 g}{\partial x^2} + \frac{\partial^2 g}{\partial y^2}\right) \quad (2)$$

Based on Eqs. (1) - (2), $\left(\frac{\partial g}{\partial x}\right)$ and $\left(\frac{\partial g}{\partial x}\right)$ represent the gradient along the $x$ and $y$ direction, signifying the interval between 2 adjacent measuring points [41]. FHD is utilized to identify subsurface lineaments deduced from the peak point of the gravity anomaly contour [42]. The SVD analysis is associated with shallow structures, characterized by a 0 point on the analysis curve. A perpendicular incision is executed on the derivative anomaly map, aligning with the derivative analysis curve output. The fault's location is deduced by referencing the FHD curve's maximum point and the SVD curve's 0 point, coinciding with identical coordinates [43]. Furthermore, based on the fault location, slicing was made to model the subsurface structure based on the thickness of the rock formation and rock density. Data processing was started by creating Bouguer anomaly maps using Oasis Montaj software. Then, modelling was done to obtain 2-dimensional profiles using GYM-SYS software in Oasis Montaj.

## Results and discussion

### Complete bouguer anomaly

The result of gravity data processing from the distribution of anomaly Bouguer shows anomaly variations based on the geology of the study area. The Complete Bouguer Anomaly (CBA) is categorized into 2 distinct types, low anomaly and high anomaly, based on their contrast. The low anomaly in the northern region corresponds to the peak of Semeru volcano, which is indicated by a blue color. This is interpreted to represent the location of an active magma chamber. The high anomaly areas, illustrated in red and extending from the east to the southwest, are presumed to represent Mount Semeru's frozen lava, indicative of dense and extensive igneous rock formations [44].

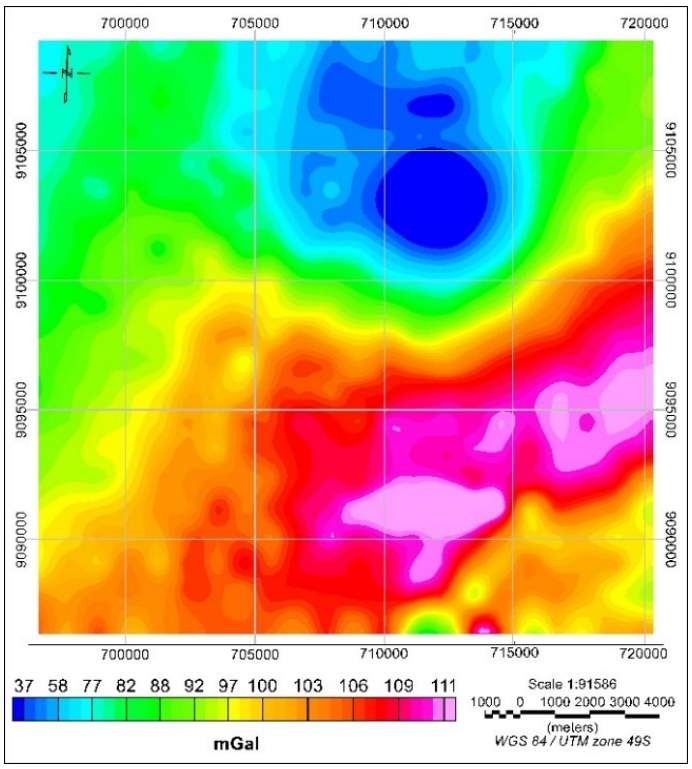


**Figure 3** Complete Bouguer Anomaly (CBA) contour map distributed on a horizontal surface.

**Separate residual anomaly**

Spectrum analysis is performed to distinguish between regional and residual anomalies, utilizing an upward continuation filter for this separation. The principle of this filter is to weaken the effect of shortwave anomalies (residual anomalies), amplify the effect of longwave anomalies (regional anomalies) and elimate noise from objects near the surface. In the radial average spectrum curve (**Figure 4**), according to the formula [40], the black circle in the upper part indicates a regional anomaly. The red color identifies the residual anomaly characterized by the line equation A = − 8.5497k + 0.9066, so the residual depth obtained is 1.3 km or deeper. The black circle in the lower part also represents the noise.

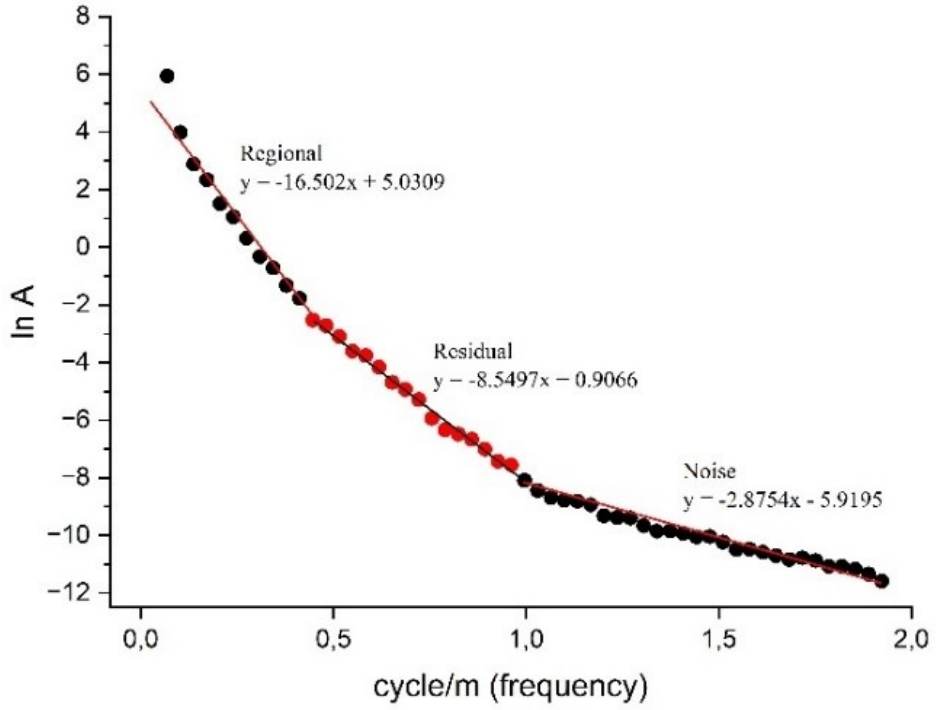


**Figure 4** Radial average power spectrum graph of the Bouguer anomaly divided into 3 anomaly sections. The straight line represents a linear function to determine the depth of each anomaly.

The residual anomaly in this research shows anomaly contrasts confirmed as rock formation boundaries (**Figure 5**), in alignment with the regional geologic map [35]. The contrasting boundaries of low and high anomalies signify lithological contacts between subsurface rock units. The low anomaly in the north is predicted to result from a combination of the Qvs and Qvj formation. Volcanic clastics characterize the Qvs formation, whereas the Qvj formation comprises basaltic lava, tuff and sand. The high anomaly in the east is attributed to the Tmw and Tomm formations, dating from the late Oligocene to the middle Miocene. The Mandalika Formation includes andesitic lava and breccia, while the Wuni Formation predominantly features breccia. The most visible anomaly contrast pattern is in the southeast, with a northeast-southwest orientation in the black box. This pattern is influenced by shifting rock contacts or faults, creating structurally weak zones within the fault areas [3]. However, precisely identifying geological structures based solely on the anomaly map is challenging [45,46], necessitating derivative analysis to enhance interpretation clarity.

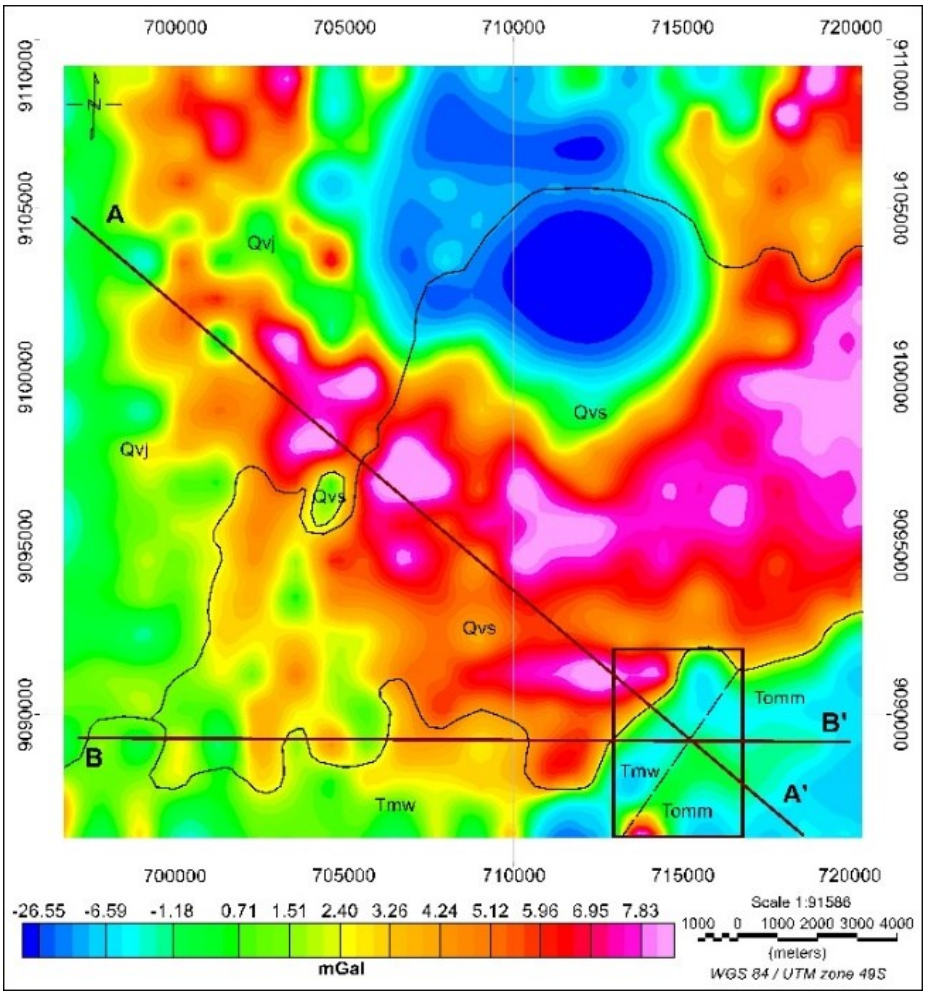


**Figure 5** Contour map of anomaly residual. The black line corresponds to the lithological boundary based on the geological map [35]. The black box represents the estimated fault. The dashed black line is slicing for subsurface structure modeling.

**Derivative analysis**

The fault location is confirmed through the analysis of FHD and SVD data. The fault structure is identified at the FHD's maximum value, depicted in red and the SVD's 0 value, positioned between its maximum and minimum values, illustrated in white. Thus, using the predicted fault zone and derivative analysis, the presumed fault structure is delineated with a black line in **Figure 6**. We conducted a derivative analysis delineation on the FHD and SVD maps to verify the fault's presence, producing a power spectrum graph (**Figure 7**) with UTM coordinates for easy tracking on FHD and SVD maps. The alignment of the FHD and SVD graphs confirms the fault's location, indicating it is consistent across both mappings. The fault structure is indicated when the incision passes through the structure boundary. The FHD curve's maximum point aligns with the SVD curve's 0 point, demonstrating a correlation between the 2.

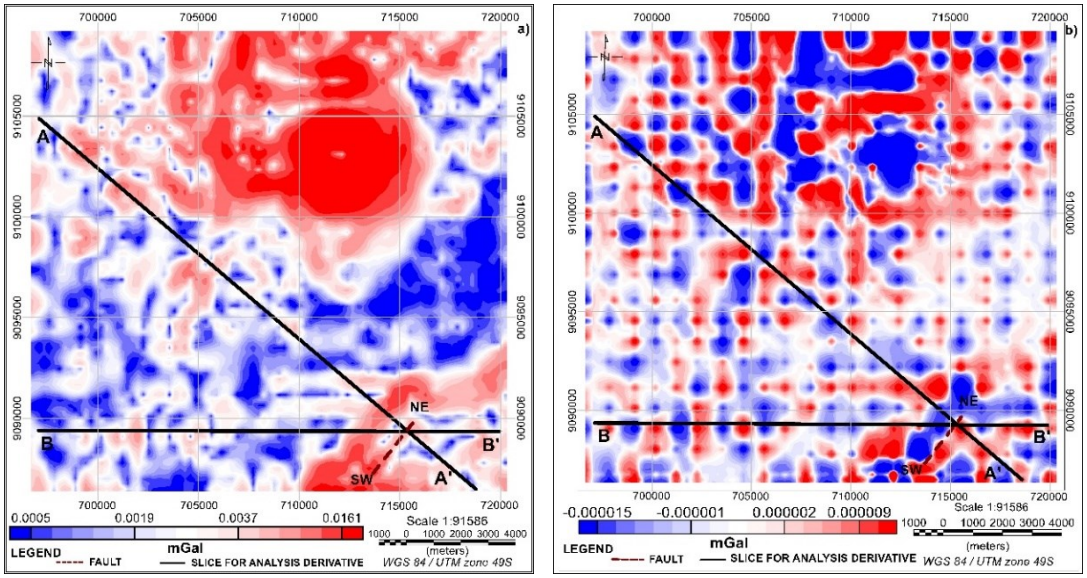


**Figure 6** Contour map at Semeru volcano (a) First horizontal derivative (left panel) and (b) Second vertical derivative (right panel). The black line represents the fault structure. The dashed brown line is an incision for subsurface structure modeling.

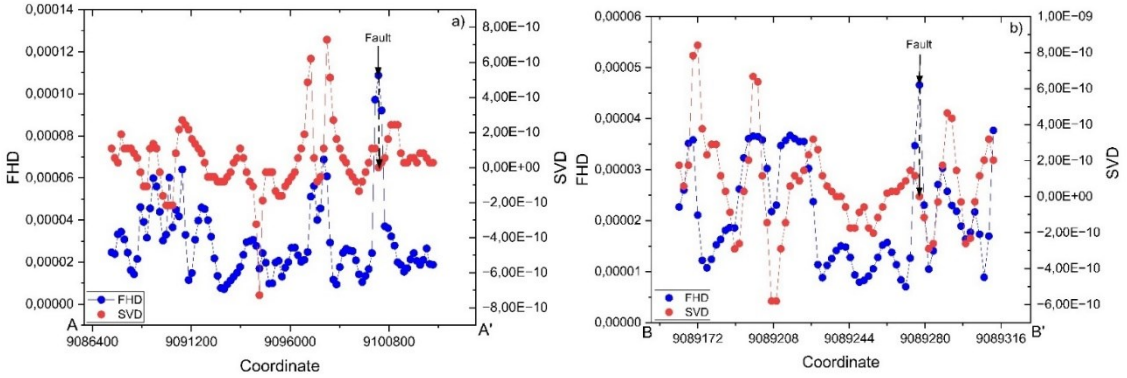


**Figure 7** Derivative analysis curves observed from the incision on FHD (blue color) and SVD (red color) maps, (a) The result of incision A-A' (upper panel) and (b) The result of incision B-B' (lower panel).

Based on **Figure 7**, the FHD and SVD curves show the presence of fault structures. The incision on the FHD curves identifies a fault zone at the maximum gravity anomaly point, signifying a significant rock density contrast in the subsurface [47]. Similarly, with the SVD curve, the presence of faults is indicated by extreme maximum and minimum anomalies with 0 point on the SVD curve. This 0 point correlates with a density contrast transition, pinpointing the anomaly source in the subsurface [48]. The maximum point on the FHD and 0 point on the SVD at the same coordinates indicate a fault zone [49]. Together, these points corroborate the presence of faults in the Semeru area, as shown by the A-A' and B-B' derivative analysis curves. The A-A' incision line demonstrates that at matching coordinates where the FHD value peaks, the SVD value is 0, a pattern also observed for B-B'. The A-A' and B-B' incision lines mutually validate the existence of a fault zone at their intersection.

**Subsurface structure model**

The model illustrates subsurface structures in distance (x) and depth (y) positions. This modeling utilizes the GM-SYS filter for forward modeling, employing residual gravity anomalies. The model verifies the presence of geological structures, delineating rock formations boundary and fault structures along with their estimated depths. Rock types were identified by analyzing the density contrasts between igneous and sedimentary rocks [50]. An incision was made across the residual anomaly profile with the same orientation and coordinates as the derivative analysis structure (**Figure 5**). An incision aligned with the orientation and coordinates of the derivative analysis structure was applied across the residual anomaly profile. The model displays the subsurface structures with reference to the geology of the Semeru volcano [51]. The cone predominantly comprises Semeru pyroclastic fall deposits, while the underlying rock formation is believed to be primarily ancient andesite [34].

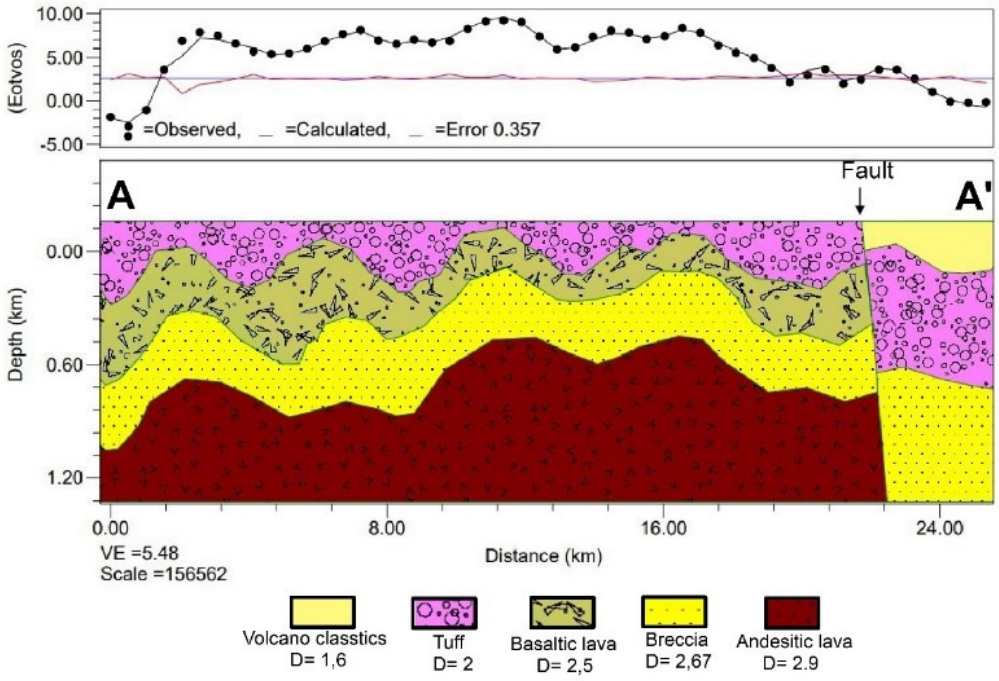


**Figure 8** Two-dimensional subsurface structure profile models of A-A' incision.

The composition trend of the component rocks depicted in **Figures 8** and **9** are consistent across both incisions, encompassing volcanic clastics, tuff, breccia and andesitic lava. However, incision A-A' has different component rocks, such as basaltic lava. In both incisions, the volcanic clastic rock formation, characterized by a low 1.6 g/cm³ density, predominates the near-surface, reaching 0.48 km above sea level in incisions A-A' and 0.36 km in B-B'. At greater depths, the increasing density values, indicative of andesitic lava's dominance, reach 2.9 g/cm$^3$ at 0.72 km below sea level in incisions A-A' and 1.2 km in incisions B-B'.

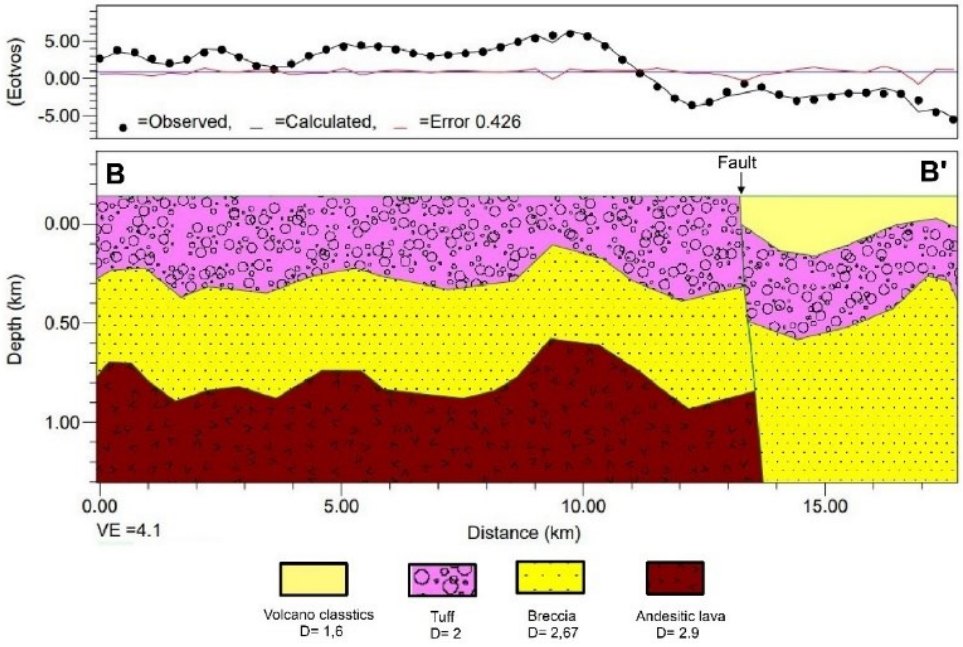


**Figure 9** Two-dimensional subsurface structure profile models of B-B' incision.

The modeling incorporates derivative analysis curves that confirm anomalies identified as faults. Referring to Sumintadireja *et al.* [48], based on the density transition in the SVD curve, the second derivative value of the maximum gravity anomaly $|g''_{max}|$ is greater than the minimum gravity $|g''_{min}|$ (**Figure 7**), the fault model is plotted with an inward sloping edge. Integrating the density values and the regional geological map [35], the fault structure modeling for the Semeru area reveals a northeast-southwest orientation.

Tectonic activity in the subduction zone located south of Java Island triggers the subsurface geological structures. Tectonic activity in the subduction zone south of Java Island instigates these subsurface geological structures, positioning the western rock blocks relatively below the fault plane (footwall) compared to those above the fault (hanging wall). This finding aligns with the geological and morphological map of Mount Semeru, showing it is largely composed of volcanic lava rock deposits [52,53]. Moreover, the Semeru/Mahameru eruption deposits, along with tuff and andesite residues from the Oligocene-Miocene period, delineate rock boundaries manifesting as normal faults due to the compression and vertical uplift of rock blocks within the subduction zone south of Java Island [36].

**Discussion**

Analyzing subsurface structures in geophysics presents a complex and time-intensive task. Utilizing satellite data-based gravity methods for subsurface structure analysis can provide quantitative insights into mass distribution variations attributable to different rock types and their material properties. The anomaly contrast indicates a low anomaly centered on Mount Semeru's summit, the lava production of young Mount Semeru.

Through subsurface estimation, GGmplus gravity data analysis can reveal the complexity of subsurface geological structures, especially fault structures. In estimating fault structures within the Semeru region, this study employs analytical methods to enhance the identification and characterization of

subsurface geological structures. Identifying geological structures is crucial due to their potential to induce geological instability.

The GGmplus data requires validation using ground-based data [54]. Hence, correlating with reference field data is essential, with this study utilizing regional geological maps from the Geological Research and Development Centre [35]. Based on **Figure 5**, contrasting high and low Bouguer anomaly transitions suggest underlying geological structures; overlaying this with a geological map delineates contact boundaries among the Wuni Formation, Mandalika, Jembangan Volcanic Quarter and Semeru volcanic Quarter. Another finding is the fault zone located southeast of the Semeru crater. Subsequent processing, including derivative analysis with perpendicular incisions, confirms this fault zone.

**Figure 7** presents a derivative analysis curve to ascertain a fault zone's presence, indicated by the maximum FHD value and 0 SVD value. Fault zones were reassessed using regional geological data for estimation. Consequently, a fault zone suggested by the derivative analysis profile curve but unverified on the regional geological map cannot be definitively classified as such. The derivative analysis curve profile and regional geological map indicate that the fault zone is positioned southeast of the Semeru peak, exhibiting a northeast-southwest orientation. A subsurface structure model was developed, incorporating rock formations and identified fault structures. As this research serves as an initial investigation, subsequent in-depth studies are required to comprehensively elucidate the subsurface geological structures. Future research could employ the magnetotelluric method to enhance the detection of anomalies suggestive of subsurface faults, utilize the geoelectrical resistivity method to delineate various rock formations beneath the surface and incorporate drill data for calibrating and validating the interpretations derived from geophysical analyses previously conducted.

## Conclusions

Residual anomalies represent rock densities at shallow depths as indicators to estimate subsurface geological structures. The residual anomaly map reveals values ranging from −26.55 (indicating low density) to 7.83 mGal (indicating high density). In the map, blue-colored areas signify low-density regions, whereas red-colored areas represent high-density regions. The transition from red to blue in the anomaly indicates the presence of geological structures, signifying contact between different rock formations and potential fault lines. The derivative analysis profile curve (FHD and SVD) fault structures, confirmed by regional geological data, identifying fault structures at 3 rock contact boundaries with a northeast-southwest orientation in Mount Semeru's southeast region. Additionally, the subsurface structure model delineates a formation composed of volcanic clastics, tuff, breccia, basaltic lava and andesitic lava extending in a southeast-west direction and a formation of 4 rock types volcanic clastics, tuff, breccia and andesitic lava in the east-west part of Mount Semeru.

## Acknowledgements

The authors are grateful to Brawijaya Volcano and Geothermal Research Center (BRAVO GRC) of Brawijaya, Malang, East Java, Indonesia and Institution of Research and Community Services of Brawijaya University (LPPM-UB), Indonesia on a Leading Research Grants Program under contract number 612.39/UN10.C20/2023 for the fund and valuable thoughts as well as the Bruce Murray Laboratory for the data used in this study available from a Global Gravity Model plus (GGMplus) satellite by California Institute of Technology (https://murray-lab.caltech.edu/GGMplus/index.html), Division of Geological & Planetary Sciences, and the USGS that has provided the SRTM DEM data for this research.

**References**

[1] A Novianto, S Sutanto, S Suharsono, C Prasetyadi and J Setiawan. Structure boundary separating using gravity data for central and southern parts of the east java basin beneath the quaternary volcanic deposits. *Iraqi Geol. J.* 2022; **55**, 1-13.

[2] H Suwargana, Z Zakaria, D Muslim, I Haryanto, EJ Wahyudi and N Rohaendi. Gravity modeling to understand the subsurface geology of the central part of West Bandung Regency (Citatah Karst Area, Cipatat-Padalarang). *Trends Sci.* 2023; **20**, 6522.

[3] C Gasston, JM Lindsay, JD Eccles, M Brook, M Hill and J Kenny. A geophysical and geomorphological investigation of large-offset normal faulting in Beachlands, Auckland. *New Zeal. J. Geol. Geophys*. 2021; **64**, 37-48.

[4] Y Ming, X Niu, X Xie, Z Han, Q Li and S Sun. Application of gravity exploration in urban active fault detection. *IOP Conf. Ser. Earth Environ. Sci.* 2021; **660**, 012057.

[5] SM Alif, EI Fattah and M Kholil. Geodetic slip rate and locking depth of east semangko fault derived from GPS measurement. *Geodes. Geodyn.* 2020; **11**, 222-8.

[6] A Susilo, Sunaryo, F Fitriah and Sarjiyana. Fault analysis in Pohgajih Village, Blitar, Indonesia using resistivity method for hazard risk reduction. *Int. J. Geomate* 2018; **14**, 111-8.

[7] C Xu. Do buried-rupture earthquakes trigger less landslides than surface-rupture earthquakes for reverse faults? *Geomorphology* 2014; **216**, 53-57.

[8] F Muttaqy, AD Nugraha, NT Puspito, DP Sahara, Z Zulfakriza, S Rohadi and P Supendi. Double-difference earthquake relocation using waveform cross-correlation in Central and East Java, Indonesia. *Geosci. Lett.* 2023; **10**, 5.

[9] S Pasari, AVH Simanjuntak, A Mehta, Neha and Y Sharma. The current state of earthquake potential on Java Island, Indonesia. *Pure Appl. Geophys*. 2021; **178**, 2789-806.

[10] A Susilo and Z Adnan. Probabilistic seismic hazard analysis of East Java Region, Indonesia. *Int. J. Comput. Electr. Eng.* 2013; **5**, 341-4.

[11] F Muttaqy, AD Nugraha, J Mori, NT Puspito, P Supendi and S Rohadi. Seismic imaging of lithospheric structure beneath Central-East Java Region, Indonesia: Relation to recent earthquakes. *Front. Earth Sci.* 2022; **10**, 756806.

[12] CCA Starheim, C Gomez, T Davies, F Lavigne and P Wassmer. In-flow evolution of lahar deposits from video-imagery with implications for post-event deposit interpretation, Mount Semeru, Indonesia. *J. Volcanol. Geoth. Res.* 2013; **256**, 96-104.

[13] N Wahyuningtyas, RP Yaniafari, F Rosyida, R Megasari, K Dewi and K Khotimah. Mapping a eruption disaster-prone area in the bromo-tengger-semeru national tourism strategic area (case study of Mount Semeru, Indonesia). *GeoJournal Tourism Geosites* 2021; **39**, 1430-8.

[14] Y Daud, A Sulistyo, F Fahmi, WA Nuqramadha, Fitrianita, RS Sesesega and S Rosid. First horizontal derivative and euler deconvolution in application for reconstructing structural signature over the Blawan-Ijen geothermal area. *IOP Conf. Ser. Earth Environ. Sci.* 2019; **2320**, 040006.

[15] R Lewerissa, N Alzair and L Lapono. Identification of ransiki fault segment in South Manokwari Regency, West Papua Province, Indonesia based on analysis of a high-resolution of global gravity field: Implications on the earthquake source parameters. *IOP Conf. Ser. Earth Environ. Sci.* 2021; **873**, 012048.

[16] MI Nurwidyanto, T Yulianto and S Widada. Modeling of Semarang Fault Zone using gravity method. *J. Phys. Conf. Ser.* 2019; **1217**, 113-9.

[17] KN Aziz, E Hartantyo and SW Niasari. The study of fault lineament pattern of the Lamongan volcanic

field using gravity data. *J. Phys. Conf. Ser.* 2018; **1011**, 012025.

[18] Supriyadi, V Soraya, A Suprianto and N Priyantari. Identification of Blawan-Ijen fault based on GGMplus gravity data using Second Vertical Derivative (SVD) analysis. *AIP Conf. Proc*. 2021; **2663**, 040005.

[19] B Legowo, R Nailatunisrina, H Purwanto, B Purnama and W Suryanto. Modelling of Volcano Lawu Fault structure using gravity anomaly to determine landslides potential. *IOP Conf. Ser. Earth Environ.* 2022; **986**, 012025.

[20] M Sutasoma, A Susilo, Sunaryo, EA Suryo and S Minardi. Analysis of the rock layer contact using the gravity data of satellite imagery and resistivity method. *Int. J. Geomate* 2022; **23**, 69-76.

[21] E Aboud, A Shareef, FA Alqahtani and S Mogren. Using a 3D gravity inversion technique to image the subsurface density structure in the Lunayyir volcanic field, Saudi Arabia. *J. Asian Earth Sci.* 2018; **161**, 14-24.

[22] A Suprianto, S Adi and BE Cahyono. Correlation between GGMPlus, Topex and BGI gravity data in volcanic areas of Java Island correlation between GGMPlus, Topex and BGI gravity data in volcanic areas of Java Island. *J. Phys. Conf. Ser.* 2021; **1825**, 012023.

[23] M Camacho and R Alvarez. Geophysical modeling with satellite gravity data: Eigen-6C4 vs. GGM Plus. *J. Eng.* 2021; **13**, 690-706.

[24] M Yanis, F Abdullah, N Zaini and N Ismail. The northernmost part of the Great Sumatran Fault map and images derived from gravity anomaly. *Acta Geophys.* 2021; **69**, 795-807.

[25] J Fang, X Caijun, Y Wen, S Wang, G Xu, Y Zhao and L Yei. The 2018 Mw 7.5 Palu earthquake: A supershear rupture event constrained by InSAR and broadband regional seismograms. *Rem. Sens.* 2019; **11**, 1330.

[26] P Omollo and J Nishijima. Analysis and interpretation of the gravity data to delineate subsurface structural geometry of the Olkaria geothermal reservoir, Kenya. *Geothermics* 2023; **110**, 102663.

[27] LT Pham, AM Eldosouky, E Oksum and SA Saada. A new high resolution filter for source edge detection of potential field data. *Geocarto Int.* 2022; **37**, 3051-68.

[28] Y Hiramatsu, A Sawada, W Kobayashi, S Ishida and M Hamada. Gravity gradient tensor analysis to an active fault: A case study at the Togi-gawa Nangan fault, Noto Peninsula, Central Japan. *Earth Planets Space* 2019; **71**, 107.

[29] MS Rosid, YH Ali and M Ramdhan. Characterization of the Mamasa earthquake source based on hypocenter relocation and gravity derivative data analysis. *Int. J. Geomate* 2022; **23**, 220-7.

[30] NAG Lestari, S Maryanto and DR Santoso. Derivative analysis for estimating subsurface structures in the kawi-songgoriti geothermal area. *AIP Conf. Proc.* 2023; **2540**, 060006.

[31] M Shimomura, WFS Banggur and A Loeqman. Numerical simulation of pyroclastic flow at Mt. Semeru in 2002. *Disast. Res.* 2019; **14**, 116-25.

[32] S Siswowidjoyo, U Sudarsono and AD Wirakusumah. The threat of hazards in the Semeru volcano region in East Java, Indonesia. *J. Asian Earth Sci.* 1997; **15**, 185-94.

[33] T Nishimura, M Iguchi, R Kawaguchi, Surono, M Hendrasto and U Rosadi. Inflations prior to vulcanian eruptions and gas bursts detected by tilt observations at Semeru Volcano, Indonesia. *Bull. Volcanol.* 2012; **74**, 903-11.

[34] A Solikhin, J Thouret, A Gupta, AJL Harris and S Chin. Geomorphology geology, tectonics, and the 2002 - 2003 eruption of the Semeru Volcano, Indonesia: Interpreted from high-spatial resolution satellite imagery. *Geomorphology* 2012; **138**, 364-79.

[35] Sujanto, Hadisantono R, Kusnama, R Chaniago and R Baharudin. *Geologic map of the Turen Quadrangle, Jawa.* Geological Research and Development Centre, Bandung, Indonesia, 1992.

[36] JC Thouret, F Lavigne, H Suwa, B Sukatja and Surono. Volcanic hazards at Mount Semeru, East Java (Indonesia), with emphasis on lahars. *Bull. Volcanol.* 2007; **70**, 221-44.

[37] M Albayrak, C Hirt, S Guillaume, K Halicioglu, MT Özlüdemir and CK Shum. Quality assessment of global gravity field models in coastal zones: A case study using astrogeodetic vertical deflections in Istanbul, Turkey. *Studia Geophys. Geodaetica* 2020; **64**, 306-29.

[38] M Akhadi, D Harahap, H Subakti and Wandono. The utilization of GGMplus data using derivative method and 3D modeling of subsurface structure for Trienggadeng fault identification in Pidie Jaya, Aceh Region. *J. Phys. Conf. Ser.* 2021; **1805**, 012037.

[39] MFR Hasan, A Susilo, EA Surto, PAM Agung, MH Idmi, DA Suaidi and F Aprilia. Mapping of landslide potential in Payung, Batu City, Indonesia, using global gravity model plus (GGMplus) data as landslide mitigation. *Iraqi Geol. J.* 2024; **57**, 159-68.

[40] H Kebede, A Alemu and S Fisseha. Upward continuation and polynomial trend analysis as a gravity data decomposition, case study at Ziway-Shala basin, central Main Ethiopian rift. *Heliyon* 2020; **2405**, e03292.

[41] RJ Blakely. *Potential theory in gravity and magnetic applications*. Cambridge University Press, Cambridge, England, 1996.

[42] MS Rosid. Determining fault structure using First Horizontal Derivative (FHD) and Horizontal Vertical Diagonal Maxima (HVDM) method: A comparative study. *AIP Conf. Proc*. 2017; **1862**, 030171.

[43] A Barkah and Y Daud. Identification of structural geologyat the Tangkuban Parahu geothermal area, West Java based on remote sensing and gravity data. *AIP Conf. Proc.* 2021; **2320**, 040006.

[44] A Realita, MN Fahmi, T Prastowo and M Madlazim. Detection of lahar flow direction from Semeru eruption on 4 December 2021 using gravity method. *J. Phys. Sci. Eng.* 2022; **7**, 75-85.

[45] BD Mulugeta, Y Fujimitsu, J Nishijima and H Saibi. Interpretation of gravity data to delineate the subsurface structures and reservoir geometry of the Aluto-Langano geothermal field, Ethiopia. *Geothermics* 2021; **94**, 102093.

[46] N Sulaiman, MM Nordiana, R Saad, M Syukri, H Hisham, U Maslinda and SR Ihsan. Gravity method used in identifying the northern part of Seulimeum Fault, Krueng Raya, Aceh Besar, Indonesia. *Electron. J. Geotech. Eng.* 2015; **20**, 4631-7.

[47] MS Rosid and H Siregar. Determining fault structure using first horizontal derivative (FHD) and horizontal vertical diagonal maxima (HVDM) method: A comparative study. *AIP Conf. Proc.* 2017; **1862**, 030171.

[48] P Sumintadireja, D Dahrin and H Grandis. A note on the use of the second vertical derivative (SVD) of gravity data with reference to Indonesian cases. *J. Eng. Tech. Sci.* 2018; **50**, 127-39.

[49] AD Hafidah, Y Daud and A Usman. Reservoir identification based on gravity method at 'aUN' geothermal field. *E3S Web Conf.* 2019; **125**, 14008.

[50] WM Telford, LP Geldart and RE Sheriff. *Applied geophysics*. Cambridge University Press, Cambridge, England, 1990.

[51] IG Sutawidjaja, D Wahyudin and E Kusdinar. *Geological map of Semeru Volcano, East Java*. Volcanological Survey of Indonesia, Bandung, Indonesia, 1996.

[52] Z Kassouk, J Thouret, A Gupta, A Solikhin and S Chin. Object-oriented classification of a high-spatial resolution SPOT5 image for mapping geology and landforms of active volcanoes: Semeru case study, Indonesia. *Geomorphology* 2014; **221**, 18-33.

[53] S Nakada, F Maeno, M Yoshimoto, N Hokanishi, T Shimano, A Zaenudin and M Iguci. Eruption scenarios of active volcanoes in Indonesia. *J. Disast. Res.* 2019; **14**, 40-50.

[54] NAZ Yahaya, AHM Din, AH Omar, NM Abdullah, NM Yazid, MF Pa'suya and MIA Wahab. Assessment of global geopotential models for modelling Malaysia marine geoid. *Int. J. Integrated Eng.* 2022; **14**, 13-24.